dramatically when considering absolute returns as a measure of volatility. Here we see that the transformed price data behave differently from their counterpart derived from the input series, and exhibit $H = 0.85$ which is a sign of strong persistence in volatility. The exponent is again very close to the scaling found for empirical data[6,20].

As these scaling properties are absent in the external driving force, they are generated by the interaction of economic agents with heterogeneous beliefs and strategies in our simulated market. Can we explain the emergence of power laws in these simulations? A closer investigation reveals that the alternation between tranquil and turbulent periods comes about through the changes of agents between groups. In particular, in periods of high volatility we also find a large fraction of agents in the noise trader group. Theoretical analysis shows that a critical value for the number of noise traders exists where the system loses its stability. Volatility is above average when the fraction of noise traders comes close to this critical point, or even increases beyond it, for some time. However, the ensuing destabilization is only temporary, and turbulent phases are overcome quickly by endogenous mechanisms: large deviations from the fundamental value are seen as profit opportunities by fundamentalists whose operations then tend to stabilize the market again. This temporal instability is similar to mechanisms found recently in various models in physics where this phenomenon has been denoted on-off intermittency[21–23]. As the possibility of temporal destabilization (with ensuing bursts of volatility) exists for an open set of parameter values, the qualitative outcome of our model seems to be extremely robust. This has been confirmed by simulations with many different parameter sets (data not shown), which all led to endogenous emergence of power-law tails and temporal dependence of volatility, albeit with varying coefficients α and H. □

Received 29 October; accepted 27 November 1998.

1. Mandelbrot, B. The variation of certain speculative prices. *J. Bus.* **35,** 394–419 (1963).
2. Fama, E. Mandelbrot and the stable Paretian hypothesis. *J. Bus.* **35,** 420–429 (1963).
3. Mantegna, R. N. & Stanley, E. Scaling behaviour in the dynamics of an economic index. *Nature* **376,** 46–49 (1995).
4. Ghashgaie, S., Breymann, W., Peinke, J., Talkner, P. & Dodge, Y. Turbulent cascades in foreign exchange markets. *Nature* **381,** 767–770 (1996).
5. Galluccio, S., Caldarelli, G., Marsili, M. & Zhang, Y.-C. Scaling in currency exchange. *Physica A* **245,** 423–436 (1997).
6. Liu, Y., Cizeau, P., Meyer, M., Peng, C.-K. & Stanley, H. E. Correlations in economic time series. *Physica A* **245,** 437–440 (1997).
7. Fama, E. Efficient capital markets: a review of theory and empirical work. *J. Fin.* **25,** 383–417 (1970).
8. Shleifer, A. & Summers, L. H. The noise trader approach to finance. *J. Econ. Perspect.* **4,** 19–33 (1990).
9. Palmer, R. G., Arthur, W. B., Holland, J. H., LeBaron, B. & Tayler, P. Artificial economic life: a simple model for a stockmarket. *Physica D* **75,** 264–274 (1994).
10. Levy, M., Levy, H. & Solomon, S. Microscopic simulation of the stock market: the effect of microscopic diversity. *J. Phys. I (France)* **5,** 1087–1107 (1995).
11. Bak, P., Paczuski, M. & Shubik, M. Price variations in a stock market with many agents. *Physica A* **246,** 430–453 (1997).
12. Caldarelli, G., Marsili, M. & Zhang, Y.-C. A prototype model of stock exchange. *Europhys. Lett.* **40,** 479–484 (1997).
13. Brock, W. & LeBaron, B. A dynamical structural model for stock return volatility and trading volume. *Rev. Econ. Stat.* **78,** 94–110 (1996).
14. Brock, W. & Hommes, C. Rational routes to randomness. *Econometrica* **65,** 1059–1095 (1997).
15. Lux, T. Time variation of second moments from a noise trader/infection model. *J. Econ. Dyn. Control* **22,** 1–38 (1997).
16. Lux, T. The socio-economic dynamics of speculative markets: interacting agents, chaos, and the fat tails of return distributions. *J. Econ. Behav. Organizat.* **33,** 143–165 (1998).
17. Guillaume, D. M. *et al.* From the bird's eye to the microscope: a survey of new stylized facts of the intra-daily foreign exchange markets. *Fin. Stoch.* **1,** 95–129 (1997).
18. Gopikrishnan, P., Meyer, M., Amaral, L. A. N. & Stanley, H. E. Inverse cubic law for the distribution of stock price variations. *Eur. Phys. J. B* **3,** 139–140 (1998).
19. Peng, C.-K. *et al.* Mosaic organization of DNA nucleotides. *Phys. Rev. E* **49,** 1685–1689 (1994).
20. Lux, T. Long-term stochastic dependence in financial prices: evidence from the German stock market. *Appl. Econ. Lett.* **3,** 701–706 (1996).
21. Platt, N., Spiegel, E. A. & Tresser, C. On-off intermittency: a mechanism for bursting. *Phys. Rev. Lett.* **70,** 279–282 (1993).
22. Haegy, J. F., Platt, N. & Hammel, S. M. Characterization of on-off intermittency. *Phys. Rev. E* **49,** 1140–1150 (1994).
23. Youssefmir, M. & Huberman, B. Clustered volatility in multiagent dynamics. *J. Econ. Behav. Organizat.* **32,** 101–118 (1997).

Supplementary information is available on *Nature*'s World-Wide Web site (http://www.nature.com) or as paper copy from the London editorial office of *Nature*.

Acknowledgements. Financial support by Deutsche Forschungsgemeinschaft, Sonderforschungsbereich 303 at the University of Bonn is acknowledged.

Correspondence and requests for materals should be addressed to T.L. (e-mail: lux@iiw.uni-bonn.de).

A single-photon turnstile device

J. Kim*, O. Benson*, H. Kan† & Y. Yamamoto*‡

** ERATO Quantum Fluctuation Project, Edward L. Ginzton Laboratory, Stanford University, Stanford, California 94305, USA*
† ERATO Quantum Fluctuation Project, Hamamatsu Photonics Inc., Hamamatsu, Shizuoka, 434-0041, Japan
‡ NTT Basic Research Laboratories, 3-1 Morinosato-Wakamiya Atsugi, Kanagawa, 243-01, Japan

Quantum-mechanical interference between indistinguishable quantum particles profoundly affects their arrival time and counting statistics. Photons from a thermal source tend to arrive together (bunching) and their counting distribution is broader than the classical Poisson limit[1]. Electrons from a thermal source, on the other hand, tend to arrive separately (anti-bunching) and their counting distribution is narrower than the classical Poisson limit[2–4]. Manipulation of quantum-statistical properties of photons with various non-classical sources is at the heart of quantum optics: features normally characteristic of fermions—such as anti-bunching, sub-poissonian and squeezing (sub-shot-noise) behaviours—have now been demonstrated[5]. A single-photon turnstile device was proposed[6–8] to realize an effect similar to conductance quantization. Only one electron can occupy a single state owing to the Pauli exclusion principle and, for an electron waveguide that supports only one propagating transverse mode, this leads to the quantization of electrical conductance: the conductance of each propagating mode is then given by $G_Q = e^2/h$ (where e is the charge of the electron and h is Planck's constant; ref. 9). Here we report experimental progress towards generation of a similar flow of single photons with a well regulated time interval.

When a light-emitting p–n junction is driven with a high-impedance constant-current source, injection of electron–hole pairs can be regulated to below the classical shot-noise limit and light with sub-shot-noise intensity fluctuations can be generated[10]. This is possible because the inelastic scattering of electrons in a highly dissipative resistor can suppress the current noise by means of the Pauli exclusion principle[11,12], and the Coulomb repulsive interaction between electrons in a p–n junction can suppress the electron injection noise by way of the collective Coulomb blockade effect[13–15]. In these squeezing experiments with a macroscopic p–n junction, however, only large numbers of photons (of the order of $\sim 10^8$) can be regulated owing to a small single charging energy.

It has been demonstrated in mesoscopic physics that an ultra-small tunnel junction regulates the electron transport one by one owing to a single charging energy that is large compared to the thermal background energy[16–18]. If such a single-electron control technique could be extended to simultaneous control of electron and hole in a p–n junction, a single photon would be regularly emitted, one by one[6].

Our single-photon turnstile device utilizes simultaneous Coulomb blockade for electrons and holes in a mesoscopic double barrier p–n junction (Fig. 1a). The structure consists of an intrinsic central quantum well (QW) in the middle of a p–n junction and the n-type and p-type side QWs isolated by tunnel barriers from the central QW. The lateral size of the device is reduced to increase the single charging energy $e^2/2C_i$, where C_i (i is n or p) is the capacitance between the central QW and the i-side QW. At a certain bias voltage V_0, the conditions for electron resonant tunnelling are fulfilled, and the mth electron can tunnel into an electron sub-band in the central QW. When the mth electron tunnels, the Coulomb repulsive interaction between electrons shifts

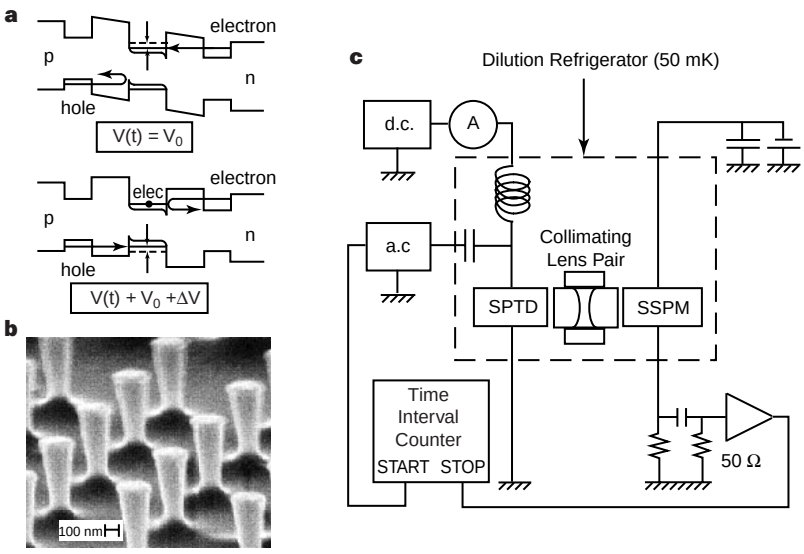

Figure 1 Operation and fabrication of our single-photon turnstile device. **a**, The operational principle of our device. When a junction voltage satisfies the electron resonant-tunnelling condition ($V = V_0$), a single (mth) electron tunnels into the central QW, and the increased Coulomb repulsive interaction between electrons prohibits subsequent electron tunnelling. Throughout the process, the hole tunnelling remains off resonant. When the junction voltage is switched to the hole resonant-tunnelling condition ($V = V_0 + \Delta V$), a single (first) hole is allowed to tunnel, but further hole tunnelling is prohibited owing to the decreased Coulomb attractive interaction between electrons and holes. Throughout this process, the electron tunnelling remains off resonant. The junction voltage is periodically modulated between these two resonant conditions so that a single electron and a single hole are injected per modulation period to produce a single photon. **b**, Scanning electron micrograph of typical etched post structures. The diameters of the devices range between 200 and 1,000 nm, and the height of the posts is ~700 nm. The junctions are located 600 nm from the top, near the bottom of the post structure. In the experiment, electrical connection is made to only one of these posts. **c**, Schematic of the experimental set-up. The fabricated single-photon turnstile device (SPTD) was installed in the mixing chamber of a dilution refrigerator at ~50 mK. The device was biased with both a d.c. and an a.c. voltage source. Photons generated from the device were focused through a collimating lens pair onto the surface of a single photon counting detector based on a solid state photomultiplier (SSPM). The temperature of the SSPM was maintained at 6.5 K with good thermal isolation. The time delay between the rising edge of the modulation input and the photon detection event was measured using a time interval counter.

the electron sub-band energy to above the Fermi level of the n-side QW, so the $(m + 1)$-th electron tunnelling is inhibited. In our single-photon turnstile device, the number of electrons in the central quantum well is $m \approx 10$ at an operating bias condition. At this bias voltage, the hole resonant-tunnelling condition is not satisfied (the Fermi level of the p-side QW is higher than the hole sub-band energy level of the central QW), so there is no hole in the central QW. Then the bias voltage is increased to $V_0 + \Delta V$ to satisfy the hole resonant-tunnelling condition. If a single hole tunnels into the hole sub-band of the central QW, the negative charge of this well is decreased by one and the subsequent hole tunnelling is inhibited owing to the decreased Coulomb attractive interaction between electrons and holes. By periodically modulating the bias voltage between V_0 and $V_0 + \Delta V$, we can inject periodically a single (mth) electron and a single (first) hole into the central QW (Fig. 1 of Supplementary Information). If the tunnel time and the radiative

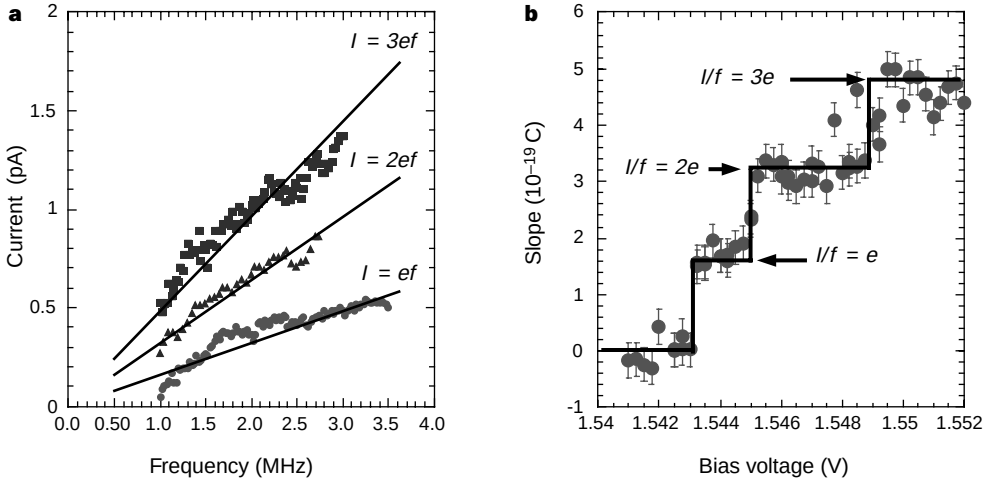

Figure 2 The electrical characteristics of the single-photon turnstile device. **a**, The modulation-frequency dependence of the direct current in the 600-nm turnstile device. A fixed a.c. amplitude of 72 mV is superposed on the three different d.c. voltages, $V = 1.545$, 1.547 and 1.550 V. The background direct (leakage) current, which is independent of the modulation frequency, has been subtracted. The measured current agrees with the relation $I = nef$ (solid lines), where e is the electron charge and $n = 1$, 2 and 3. **b**, The slopes I/f in the current–frequency curve versus d.c. bias voltage. The slopes I/f are quantized and form plateaux at multiples of e, indicating the operations at $I = ef$, $2ef$ and $3ef$.

recombination time of an electron–hole pair are much shorter than the pulse duration, one (and only one) photon is emitted for every modulation period.

A GaAs/AlGaAs three-QW structure sandwiched by n-type and p-type AlGaAs bulk layers was grown using a molecular beam epitaxy technique. Post structures with diameters of 200–1,000 nm were made by electron-beam lithography followed by metal evaporation, lift-off, and BCl_3/Cl_2 electron cyclotron resonance plasma etching. A scanning electron micrograph of typical etched posts is shown in Fig. 1b. The surface of the device was passivated with sulphur in ammonium sulphide ($(NH_4)_2S$) solution, and encapsulated by silicon nitride film[19]. The structure was covered with hard-baked photoresist and the top of the post was exposed by O_2 plasma etching. Finally, electrical connection was made to each one of the posts independently. The top semi-transparent metal served as the p-type contact from which an emitted photon is detected, and the n-type contact was formed in the substrate.

The device was installed in a dilution refrigerator with base temperature of ~50 mK, and was biased with a d.c. and an a.c. voltage source (Fig. 1c). A direct current flowing through the device was measured as a function of d.c. bias voltage with a square wave a.c. modulation voltage. The emitted photon from this device was detected by a Si solid-state photomultiplier (SSPM). This detector features a high quantum efficiency of ~88%, a high multiplication gain of ~30,000, a fast response time of ~2 ns and no multiplication noise[20]. The detector was installed on the mixing chamber of the dilution refrigerator, but the temperature was held at 6.5 K with good thermal isolation.

We measured the d.c. current–voltage characteristics and observed a well-defined resonant-tunnelling current peak with very small background current; this indicates that surface (leakage) current is well suppressed, in spite of the very small size of the post, by the above-mentioned passivation process (Fig. 2 of Supplementary Information). Measurement of the photons generated by this device indicated that the internal efficiency of photon emission from an electron-hole pair is ⩾33%.

When an a.c. modulation voltage was applied to the device in addition to the d.c. bias voltage, we observed that the direct current increased linearly as a function of the modulation frequency, f. Figure 2a shows the measured current as a function of a.c. modulation frequency, with a fixed a.c. amplitude of 72 mV at three different d.c. bias voltages for a device with a diameter of 600 nm. The measured current (I) was in close agreement with the relation $I = ef$, $I = 2ef$ and $I = 3ef$ (solid lines), when a frequency-independent background current was subtracted. This background current varies from device to device, and ranges from 0.5 to 6.5 pA. In Fig. 2b we evaluate the slope I/f from the current versus frequency curves and plot it as a function of the d.c. bias voltage. We find that the slope increases discretely, creating plateaux at $I/f = ne$, where $e = 1.6 \times 10^{-19}$ C is the charge of an electron and $n = 1$, 2 and 3.

The locking of the current at multiples of the modulation frequency ($I = nf$) suggests that the charge transfer through the device is strongly correlated with the external modulation signal[16–18]. At the first current plateau at $I = ef$, a single (mth) electron and a single (first) hole are injected into the central QW per modulation period, resulting in single-photon emission. At the second current plateau at $I = 2ef$, two (mth and $(m + 1)$-th) electrons and two (first and second) holes are injected into the central QW per modulation period, resulting in up to two-photon emission (Fig. 3 of Supplementary Information). Similarly, at the third current plateau at $I = 3ef$, three electrons and three holes are injected per modulation period, resulting in up to three-photon emission. This multiple charge operation becomes possible because of the relatively broad inhomogeneous linewidths of the n-side and

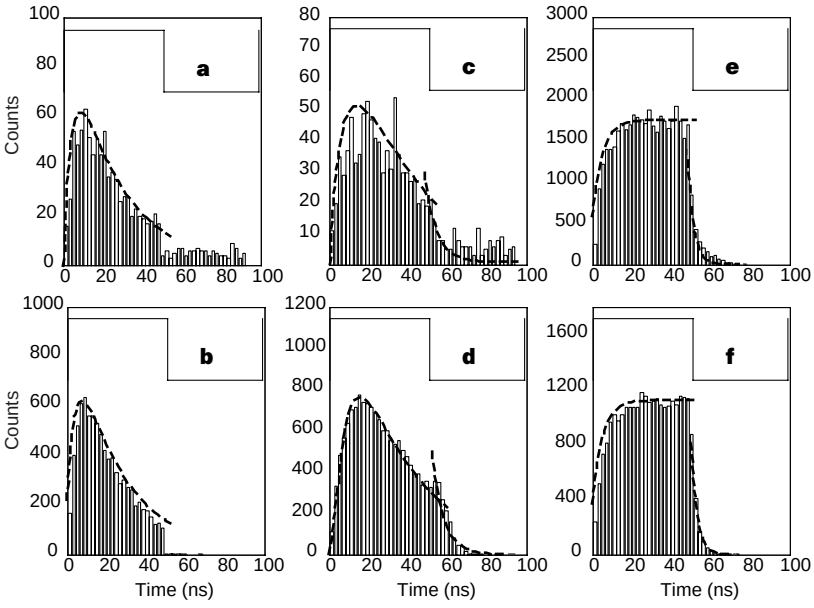

Figure 3 The photon emission characteristics of the single-photon turnstile device. **a**, Histogram of the measured time delay between the rising edge of the modulation input and the photon detection event at the first plateau ($I = ef$). The solid line at the top indicates the external a.c. modulation voltage. As a single electron is injected at V_0 and a single hole is injected at $V_0 + \Delta V$, a photon is emitted after the rising edge of the pulse. The dashed line is an analytical solution (see text). The finite photon counts during the off-pulse period are due to the dark counts of the Si SSPM. **b**, Results of a Monte-Carlo numerical simulation for the photon emission probability versus the time delay at the first plateau ($I = ef$). **c**, Measured histogram of the time delay at the second plateau ($I = 2ef$). The distribution is broader, as two electrons and two holes are injected, and up to two photons are generated per modulation period. The two dashed lines are the theoretical solutions (see text). The sharp cut-off of photon emission after the falling edge of the modulation input is due to the decay of the hole population due to simultaneous electron–hole recombination and reverse hole tunnelling. **d**, As **b**, but for the second plateau. **e**, Measured histogram of the time delays for a larger-area device (diameter, 1.4 μm) at a higher temperature (4 K), where the Coulomb blockade effect is absent. The recombination time is shorter in this case (~5 ns) due to higher carrier density at the operating condition. **f**, Monte-Carlo numerical simulation result for this case of a modulated classical light-emitting diode.

p-side QWs. The experimental results were well reproduced by Monte-Carlo numerical simulations with a finite resonance linewidth (data not shown).

To observe the temporal correlation between the modulation input and photon emission, we measured the time delay from the rising edge of the modulation input to the photon detection event at the first current plateau ($I = ef$) and at the second current plateau ($I = 2ef$). The probability of a single electron–hole pair injected to the central QW of the turnstile device being detected as a photon in the detector was $\sim 1 \times 10^{-4}$ owing to a poor optical coupling efficiency between the two devices in the present set-up. However, the detection quantum efficiency does not affect the time correlation characteristics. Histograms of the measured time delay with 10-MHz modulation frequency are shown in Fig. 3a (for $I = ef$) and Fig. 3c (for $I = 2ef$). The photon emission probabilities have peaks near the rising edge of the modulation input. The rapid increase of the photon emission probability is associated with the hole tunnelling time ($\tau_h \approx 4$ ns), and the slow decay of the photon emission probability corresponds to the electron–hole recombination lifetime ($\tau_{ph} \approx 25$ ns: due to both radiative and non-radiative processes). The photon emission probability in Fig. 3a decays to a non-zero value during the on-pulse due to photons generated by background current. The ratio of the counts contained in the peak to those contained in the non-zero background is ~3:1, consistent with the ratio of the turnstile current to the background current in this device. The second and faster decay for $I = 2ef$ (Fig. 3c) represents the decay of the hole via backward tunnelling and electron–hole recombination. The associated lifetime for this decay is $(\tau_h^{-1} + \tau_{ph}^{-1})^{-1}$. The dashed lines show the analytical solutions using these parameters.

The experimental results, as well as the analytical traces, are well reproduced by Monte Carlo numerical simulations, as shown in Fig. 3b ($I = ef$) and Fig. 3d ($I = 2ef$). The fact that the photon emission probability decreases during the duration of the on-pulse is a unique indication that the number of holes injected during an on-pulse is restricted to either one or two due to the Coulomb blockade effect (Fig. 4 of Supplementary Information). Figure 3e shows the experimental result for a larger-area device at a higher temperature of 4 K, where the Coulomb blockade effect is absent. In this case, arbitrary numbers of holes are allowed to tunnel into the central QW during an on-pulse, and so the resulting photon emission probability should increase monotonically with a time constant τ_{ph} to the steady-state value. This result is well-reproduced by the simulation (Fig. 3f).

The experimental results reported here provide evidence for the long-sought generation of regulated streams of single photons (and n-photons) where the time interval between single photons is regulated to beyond the Poisson limit. If the un-regulated background photons were suppressed and the collection efficiency was improved, such a non-classical photon source could provide an efficient source for future quantum information technologies, and could also be a useful tool for fundamental tests of quantum mechanics. □

Received 5 August; accepted 7 December 1998.

1. Hanbury Brown, R. & Twiss, R. Q. Correlation between photons in two coherent beams of light. *Nature* **177,** 27–29 (1956).
2. Reznikov, M., Heiblum, M., Shtrikman, H. & Mahalu, D. Temporal correlation of electrons: suppression of shot noise in a ballistic quantum point contact. *Phys. Rev. Lett.* **75,** 3340–3343 (1995).
3. Kumar, A., Saminadayar, L., Glattli, D. C., Jin, Y. & Etienne, B. Experimental test of the quantum shot noise reduction theory. *Phys. Rev. Lett.* **76,** 2778–2781 (1996).
4. Liu, R. C., Odom, B., Yamamoto, Y. & Tarucha, S. Quantum interference in electron collision. *Nature* **391,** 263–265 (1998).
5. Walls, D. F. & Milburn, G. J. *Quantum Optics* (Springer, Berlin, 1994).
6. Imamoğlu, A. & Yamamoto, Y. Turnstile device for heralded single photons: Coulomb blockade of electron and hole tunneling in quantum confined p–i–n heterojunctions. *Phys. Rev. Lett.* **72,** 210–213 (1994).
7. Imamoğlu, A., Schmidt, H., Woods, G. & Deutsch, M. Strongly interacting photons in a nonlinear cavity. *Phys. Rev. Lett.* **79,** 1467–1470 (1997).
8. Yamamoto, Y. A photon in solitary confinement. *Nature* **390,** 17–18 (1997).
9. von Klitzing, K., Dorda, G. & Pepper, M. New method for high-accuracy determination of the fine-structure constant based on quantized Hall resistance. *Phys. Rev. Lett.* **45,** 494–497 (1980).
10. Yamamoto, Y. in *Quantum Optics of Confined Systems* (eds Ducloy, M. & Bloch, D.) 201–281 (Kluwer, Dordrecht, 1996).
11. Beenakker, C. W. J. & Büttiker, M. Suppression of shot noise in metallic diffusive conductors. *Phys. Rev. B* **46,** 1889–1892 (1992).
12. Liu, R. C. & Yamamoto, Y. Suppression of quantum partition noise in mesoscopic electron branching circuits. *Phys. Rev. B* **49,** 10520–10532 (1994).
13. Imamoğlu, A. & Yamamoto, Y. Noise suppression in semiconductor p–i–n junctions: Transition from macroscopic squeezing to mesoscopic Coulomb blockade of electron emission process. *Phys. Rev. Lett.* **70,** 3327–3330 (1993).
14. Kim, J., Kan, H. & Yamamoto, Y. Macroscopic Coulomb-blockade effect in a constant-current-driven light-emitting diode. *Phys. Rev. B* **52,** 2008–2012 (1995).
15. Kim, J. & Yamamoto, Y. Theory of noise in p–n junction light emitters. *Phys. Rev. B* **55,** 9949–9959 (1997).
16. Delsing, P., Likharev, K. K., Kuzmin, L. S. & Claeson, T. Time-correlated single-electron tunneling in one-dimensional arrays of ultrasmall tunnel junctions. *Phys. Rev. Lett.* **63,** 1861–1864 (1989).
17. Geerligs, L. J. *et al.* Frequency-locked turnstile device for single electrons. *Phy. Rev. Lett.* **64,** 2691–2694 (1990).
18. Kouwenhoven, L. P. *et al.* Quantized current in a quantum-dot turnstile using oscillating tunnel barriers. *Phy. Rev. Lett.* **67,** 1626–1629 (1991).
19. Hobson, W. S. *et al.* Silicon nitride encapsulation of sulfide passivated GaAs/AlGaAs microdisk lasers. *J. Vac. Sci. Technol. A* **13,** 642–645 (1995).
20. Kim, J., Yamamoto, Y. & Hogue, H. H. Noise-free avalanche multiplication in Si solid state photomultipliers. *Appl. Phys. Lett.* **70,** 2852–2854 (1997).

Supplementary information is available on *Nature*'s World-Wide Web site (http://www.nature.com) or as paper copy from the London editorial office of *Nature*.

Acknowledgements. We thank H. H. Hogue for providing us with SSPM detectors. This work was partially supported by JSEP.

Correspondence and requests for materials should be addressed to Y.Y. (yamamoto@loki.stanford.edu).

Modulated phases and proton centring in ice observed by X-ray diffraction up to 170 GPa

Paul Loubeyre*†, René LeToullec†, Elodie Wolanin†, Michel Hanfland‡ & Daniel Hausermann‡

** Laboratoire Etats Extrêmes Statiques, SPMC/DPTA, CEA 91680 Bruyères-le-Châtel, France*

† CNRS and Université Paris 6, PMC boite 77, 4 place Jussieu 75252 Paris, France

‡ ESRF, BP 220, 38043 Grenoble, France

Because of its open hydrogen-bonded structure, ice shows many structural changes between different crystalline forms under high pressure. Crystallographic studies of these transitions have been pursued largely by neutron scattering, which allows the positions of the hydrogen atoms to be identified[1,2]. Such studies have previously been extended to pressures of up to 20 GPa, which is however insufficient to permit the investigation of ice X, a 'symmetric ice' in which the protons are thought to reside midway between the oxygen atoms[3–5]. So far, information about ice X has therefore come from indirect methods such as infrared[6,7] or Brillouin[8] spectroscopy. Here we show that single-crystal X-ray diffraction is able to reveal the signature of hydrogen-bond symmetrization. The 111 reflection can be assigned to the hydrogen atoms alone, and we can measure it up to 170 GPa in a diamond anvil cell. This diffraction line (normalized against the intensity of the 222 line, which is due mostly to oxygen atoms) indicates that the proton centring in ice X occurs from about 60 to 150 GPa; at this latter pressure the intensity increases sharply, signalling a further structural change. At lower pressures, we see ice VII ordering in a sequence of spatially modulated phases between 2.2 and 25 GPa, which suggests an analogy with the incommensurate phases of the frustrated Ising model[9].

We use the single-crystal X-ray diffraction technique with the high brilliance of the European Synchrotron Radiation Facility to measure the structural properties of ice VII in a diamond anvil cell at very high pressure, as described previously for solid hydrogen[10]. Ice VII is the stable form of ice at ambient temperature above 2.2 GPa, but its detailed nature remains unknown, with possible multisite disorder of both the oxygen and hydrogen atoms[2]. The single crystal was grown by looking optically at the solid–fluid